Available online at www.sciencedirect.com
ScienceDirect
NDT&E International 40 (2007) 315–323
NDT&E international
www.elsevier.com/locate/ndteint

Real-time arc-welding defect detection and classification with principal component analysis and artificial neural networks

J. Mirapeix*, P.B. García-Allende, A. Cobo, O.M. Conde, J.M. López-Higuera

Grupo de Ingeniería Fotónica; Dep.. T.E.I.S.A., Universidad de Cantabria, Avda. Los Castros s/n, 39005 Santander, Spain

Received 9 February 2006; received in revised form 5 October 2006; accepted 6 December 2006
Available online 5 February 2007

Abstract

A novel system which allows arc-welding defect detection and classification is presented in this paper. The spectroscopic analysis of the plasma spectra produced during the welding process is a well-known technique to monitor the quality of the resulting weld seams. The analysis of specific emission lines and the subsequent estimation of the electronic temperature T_e profile offers a direct correlation between this parameter and the corresponding weld seams. However, the automatic identification and classification of weld defects has proven to be difficult, and it is usually performed by means of statistical studies of the electronic temperature profile. In this paper, a new approach that allows automatic weld defect detection and classification based in the combined use of principal component analysis (PCA) and an artificial neural network (ANN) is proposed. The plasma spectra captured from the welding process is processed with PCA, which reduces the processing complexity, by performing a data compression in the spectral dimension. The designed ANN, after the selection of a proper data training set, allows automatic detection of weld defects. The proposed technique has been successfully checked. Arc-weld tests on stainless steel are reported, showing a good correlation between the ANN outputs and the classical interpretation of the electronic temperature profile.

Keywords: Spectroscopy; Plasma emission; Arc welding; PCA; Artificial neural network

1. Introduction

Although different welding processes have been used for years in various industrial applications, the introduction of arc and laser welding in the aerospace, automotive and nuclear sectors, among others, has led to a great effort in research concerning the quality assurance of those processes. The complexity of the physics involved in arc welding [1], where several input (gas flux, welding intensity, welding speed, material composition, arc length, etc.) and output parameters (weld seam geometry, weld seam quality) are interrelated by a highly non-linear and strongly-coupled process [2], makes it difficult to find a valid theoretical model to describe this kind of process. These specific characteristics of the arc-welding processes make artificial neural networks (ANN) a highly suitable solution to solve the lack of mathematical foundation for the arc-welding process. In several papers, different ANN topologies have been proposed to establish a correlation between some input welding parameters and, commonly, the weld pool geometry or the seam penetration [3–5].

The above-mentioned lack of mathematical formulation has forced to perform procedure trials in an attempt to ensure welding quality by using some specific welding parameters for given conditions. However, several disturbances can appear during the welding processes, affecting the resulting quality of the welds. The common approach to validate welding quality is performed by means of off-line destructive (macrographs) and non-destructive testing (NDT) (x-ray, ultrasounds, penetrant liquids, magnetic particles, etc.), which are expensive and time consuming techniques.

The use of an on-line, real-time welding monitor system able to detect instabilities affecting the welding quality and even to supervize the entire system to prevent these possible defects from happening would be a great asset. Spectroscopic analysis of the plasma [6,7], analysis of the acoustic

*Corresponding author. Tel./fax: +34 942200877.
E-mail address: mirapeixjm@unican.es (J. Mirapeix).

0963-8695/$ - see front matter © 2007 Published by Elsevier Ltd.
doi:10.1016/j.ndteint.2006.12.001

emission produced during the process [8] or machine vision of the weld pool [9] are some proposals which have proved their suitability to monitor welding processes. However, the direct interpretation of the results offered by these solutions tends to be difficult, and, again, ANNs have been used to identify and detect disturbances along the weld seam, like fluctuations in the bead width [4], or gap and misalignments in laser welding [10].

In this paper a new system able to detect and classify defects in arc-welding processes is presented. The plasma spectra captured during the welding tests are processed by means of *principal component analysis* (PCA) and, then, used as the input of a back propagation ANN. The selection of a proper training set for the ANN will allow the subsequent correct classification of the welding quality. Tests performed with stainless steel plates show the feasibility of the proposed solution to operate as a real-time on-line weld quality monitor system. The outputs of the designed ANN are successfully compared with electronic temperature T_e experimental profiles.

2. Plasma spectroscopy

The spectroscopic analysis of the plasma in welding processes is commonly performed by estimating the plasma electronic temperature T_e, as it has been demonstrated that a correlation exists between T_e and the welding quality [11]. The calculation of T_e from some specific plasma emission lines is derived from the Boltzmann equation:

$$N_m = \frac{N}{Z} g_m \exp\left(\frac{-E_m}{kT_e}\right), \tag{1}$$

where the population (N_m) of an excited level m can be determined when the population density N, the partition function Z, the statistical weight g_m and the excitation energy E_m are known, while k is the Boltzmann constant.

Eq. (1) is valid when the plasma is in local thermal equilibrium (LTE) [11]. If the plasma is also optically thin, then the intensity of an emission line I_{mn} can be obtained using

$$I_{mn} = N_m A_{mn} h\gamma_{mn}, \tag{2}$$

where A_{mn} is the transition probability (from the state m to n), and $h\gamma_m$ the energy of the transition (h is the Planck's constant and γ_{mn} the frequency associated to the emission line). The combination of Eqs. (1) and (2) leads to Eq. (3), which can be used to obtain T_e from a set of known emission lines:

$$\ln\left(\frac{I_{mn}\lambda_{mn}}{A_{mn}g_m}\right) = \ln\left(\frac{hcN}{Z}\right) - \frac{E_m}{kT_e}, \tag{3}$$

where λ_{mn} is the emission line central wavelength and c the light velocity. Although it has been demonstrated that the estimation of T_e obtained from (3) can offer valuable information about the welding process, it is still unclear which set of lines is the proper one to be used considering the material to be welded, the shielding gas, the specific welding conditions and the defects to be identified. A method capable of analyzing the whole spectrum, not only some particular selected emission lines, would be more robust and generic. However, the amount of information to process, considering a real-time system, could be a major drawback. For example, the spectral information to process within the proposed system consists of 2048 wavelengths (number of pixels of the spectrometer's CCD used in our setup), with an average of 50 spectra captured per second.

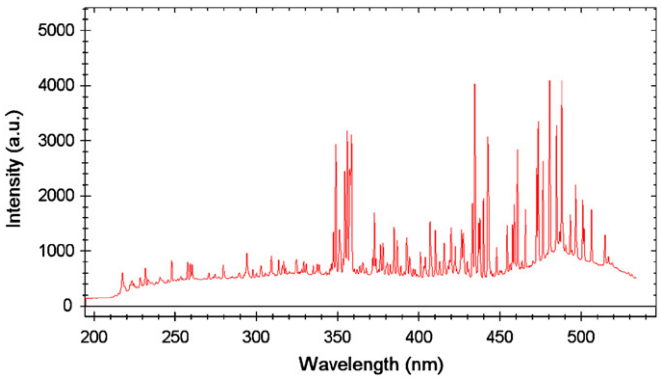

Fig. 1. Example of plasma spectrum emitted during the arc-welding process.

An example of a typical plasma spectrum captured during an arc-welding process is presented in Fig. 1. It can be seen that, between approximately 210 and 520 nm there are several emission lines which need to be accurately identified to be considered for the T_e estimation process. The approach proposed in the present paper is to use an ANN to obtain valuable information directly from the plasma spectra. This solution allows the elimination of several processing stages to be considered when an accurate T_e estimation is desired, as background suppression, peak detection, modeling and identification, among others. The computational cost of processing a large amount of data is avoided by using PCA, which compresses the input spectra in the wavelength dimension. Besides, ANNs are known to be highly computationally efficient once the network has been correctly trained.

3. Spectral software processing

The spectral interpretation process determines if each captured spectrum corresponds to a correct welding or if a defect has occurred. In the latter case, the classification system is able to distinguish between different kinds of defects. The implemented algorithm has two stages: *principal component analysis* (PCA) [12] is first used to perform simultaneously a dimensional reduction and redundancy elimination. Secondly, an ANN [13,14] is employed for the welding fault identification task. Both units will be thoroughly described in the next lines. A block-diagram of the proposed spectral analysis is depicted in Fig. 2.

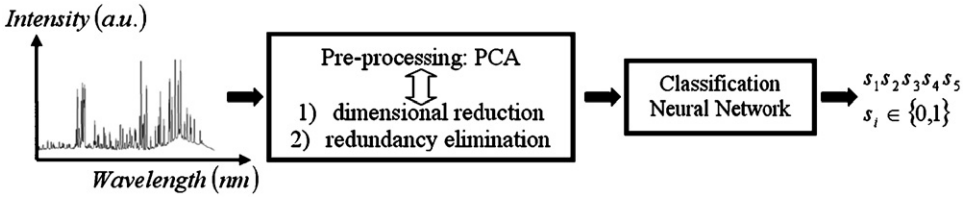

Fig. 2. Spectral analysis processing scheme.

3.1. Principal component analysis

Plasma spectrum contains redundant information for the training of the ANN due to the large amount of spectral lines to be found within the selected spectral range. Redundancy removal and data compression are performed simultaneously by means of PCA. Applying data compression implies reducing the number of required components, as much as possible, without losing relevant information. This is accomplished by the expression of the captured spectra in a different vectorial basis which is obtained in such a way that the new basis vectors are those directions of the data which contains the most relevant information. PCA assumes linearity, so the new basis is a linear combination of the original. This assumption really simplifies the problem since it restricts the set of possible new bases. X is the original data set, a $m \times n$ matrix, where m is the number of measurement types or spectral bands and n the number of samples or measured spectra. The goal of PCA is to find some orthonormal matrix P where the compressed data $Y = PX$ such that the covariance matrix of the compressed data $C_Y = \frac{1}{n-1} YY^{\mathrm{T}}$ is diagonalized. This means that the compressed data is uncorrelated. The rows of P are the *principal components* of X.

If C_Y is rewritten in terms of P:

$$C_Y = \frac{1}{n-1} YY^{\mathrm{T}} = \frac{1}{n-1} PXX^{\mathrm{T}}P^{\mathrm{T}} = \frac{1}{n-1} PAP^{\mathrm{T}}. \quad (4)$$

Since the new matrix $A \equiv XX^{\mathrm{T}}$ is symmetric, it is diagonalized by an orthogonal matrix of its eigenvectors:

$$A = EDE^{\mathrm{T}}, \quad (5)$$

where D is a diagonal matrix and E is a matrix of eigenvectors of A arranged as columns. The matrix P is selected to be a matrix where each row p_i is an eigenvector of XX^{T}. By this selection $P \equiv E^{\mathrm{T}}$ so $A = P^{\mathrm{T}}DP$. With this relation, and considering that the inverse of an orthogonal matrix is its transpose [15], C_Y is

$$C_Y = \frac{1}{n-1} PAP^{\mathrm{T}} = \frac{1}{n-1} P(P^{\mathrm{T}}DP)P^{\mathrm{T}} = \frac{1}{n-1} (PP^{-1})D(PP^{-1}) = \frac{1}{n-1} D. \quad (6)$$

It is evident that the choice of P diagonalizes C_Y and the ith diagonal value of C_Y is the variance of X along p_i and it is equal to the eigenvalue β_i. Therefore the goal of PCA is reached. In practice, computing PCA of a data set X entails subtracting off the mean of each measurement type because of the assumption of PCA that variance means information.

Once the eigenvectors have been found the input data can be transformed. Performing dimensional reduction implies ignoring some eigenvectors. The tradeoff between the wanted low dimension and the unwanted loss of information can be defined as [16]

$$I_K = \frac{\sum_{i=1}^{K} \beta_i}{\sum_{i=1}^{m} \beta_i} \cdot 100\%, \quad (7)$$

where K denotes the number of eigenvectors that is used, m denotes the dimension of the input data and I_K is the percentage of information (variance) that is kept in the compression.

Designing the spectral interpretation algorithm requires the division of the original data set into two subsets. The first one is called the training data set and it is used to obtain the vectors of the new basis using PCA and to train the ANN. These vectors are stored to be used afterwards to express the spectra in the second subset, the test data set, in this new basis. How PCA is applied to this work is summarized in Fig. 3.

Initially, the captured spectra lie in a 2048-dimensional space. The dimension of each input spectrum is reduced to 14 wavelengths by ignoring those eigenvectors whose associated eigenvalues are smaller than a thousandth of the maximum eigenvalue. This threshold is selected according to a tradeoff between the compression rate and the classification error, and it implies rejecting directions that contribute less than 0.1% to the total variation in the data set. A data compression rate of the 99% is achieved. This reduction allows a great enhancement in computational performance of the spectral interpretation algorithm, so the classification can be accomplished in real-time, without causing an appreciable increase in the error probability.

3.2. Welding fault diagnosis using artificial neural networks

An ANN able to detect, with the appropriate training, the presence of four different kinds of welding defects along the weld seam has been developed. The ability of ANNs to handle non-linearity, their parallel processing of information and their quick adaptability to system dynamics have turned out to be very useful in these applications, as the welding process depends on several different parameters. The considered welding defects are:

slight lack of penetration, lack of penetration, low welding current and inert gas flow reduction. Therefore, the data set consists of plasma spectra produced during different welding experiments, which combine correct welds with all the possible defects.

The topology and desired outputs of the network are illustrated in Fig. 4. A multilayer feed-forward network and back-propagation learning algorithm have been selected. The error considered in the training phase is defined as the mean square error between the current outputs of the ANN and the desired outputs for the training spectra. During the training stage spectra of correct welds and all the possible defects were input to the neural network. In this step the network iteratively adjusts its parameters (weights and biases) in order to produce an output that matches the results depicted in Fig. 4 for each of the considered cases. 541 spectra of correct welds, 197 of lack of penetration, 22 of low

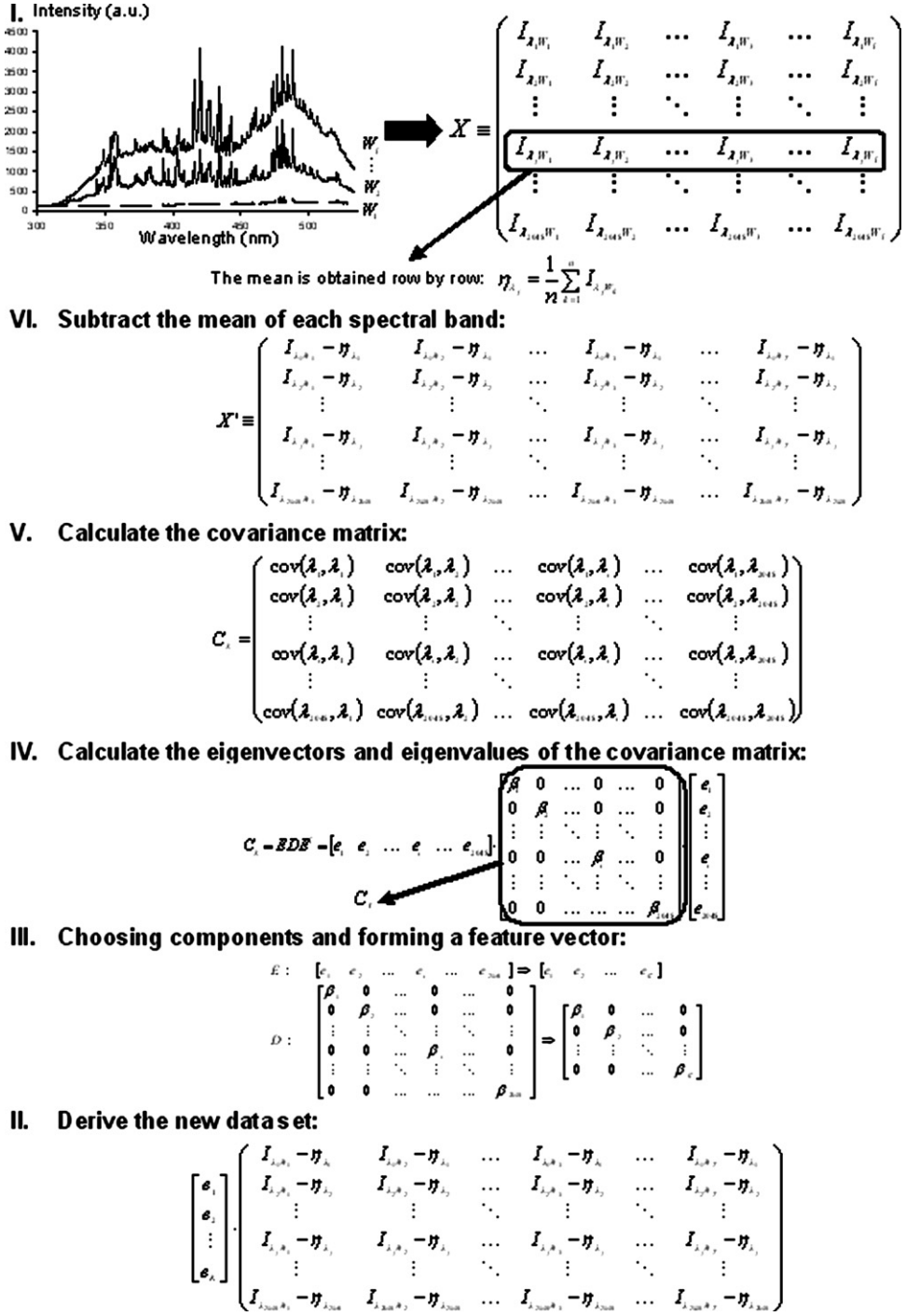

Fig. 3. Schematic description of PCA application to the captured spectra.

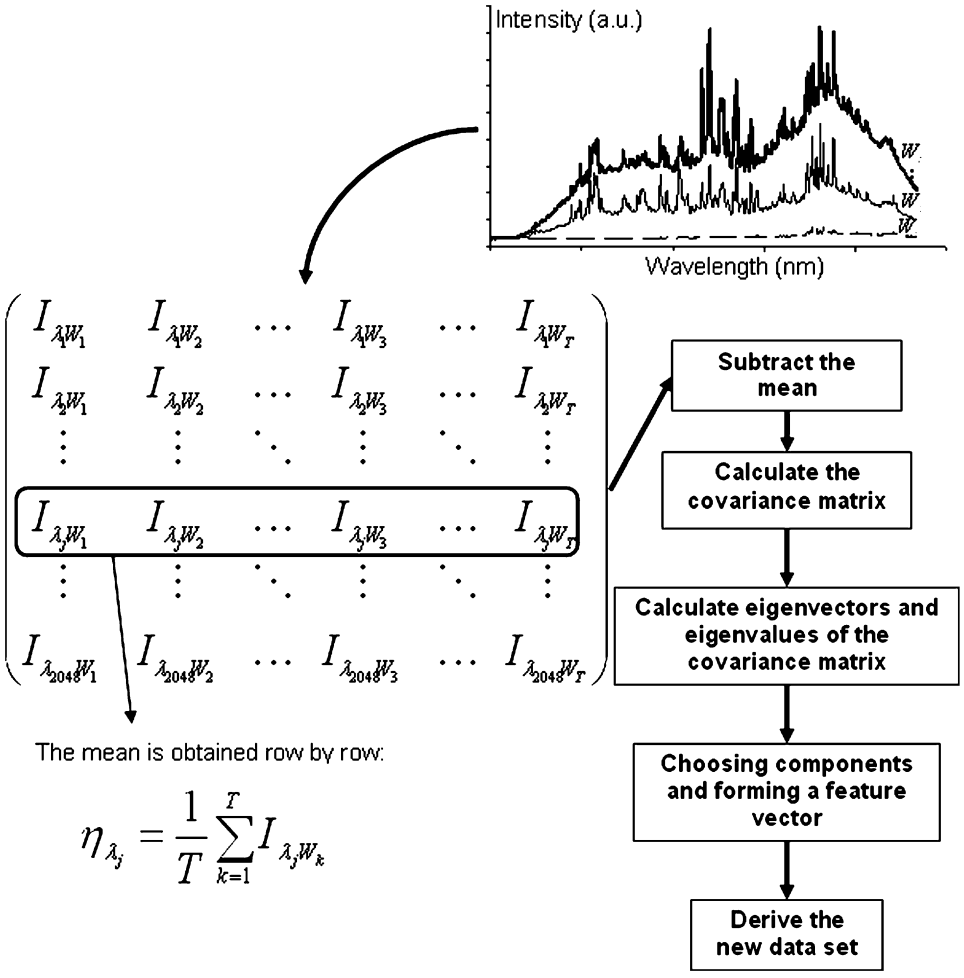

Fig. 3. (*Continued*)

welding current, 7 of inert gas flow reduction and 66 of slight lack of penetration are employed and the goal error selected in this training phase was 0.001%. The appropriate number of hidden layers and the number of neurons or processing elements of all of them have been experimented in the test phase. Different ANN topologies with one and two hidden layers and with a number of neurons in each layer from 30 to 50 were tested. The purpose of this study was to obtain the best network topology in terms of simplicity and minimization of the classification error. The classification error percentage introduced by the ANN in the test data set is used as a measurement of the goodness of the designed net structure. Finally, the net consists of an input layer and two hidden layers, the three of them with 50 neurons, and an output layer with only 5 neurons, corresponding to the correct welds and the above mentioned classification of weld faults. The neurons in all layers have a log-sigmoid transfer function.

The processing scheme detailed in Fig. 2 has been checked with several tests. The experimental setup and results provided by the classification algorithm will be presented in the next section.

4. Experimental setup and results

A schematic description of the experimental setup used to perform TIG welds is presented in Fig. 5. The welding system is formed by a "Kemppi Mastertig 2200" power source, a welding torch that remains fixed and a high-precision positioning system with two linear stages (Newport MTM100PP1) of 1 μm resolution. The AISI-304 stainless steel plates(1 mm thickness) used in the experiments were fastened to the positioning system, controlled by a Newport MM4005 controller. The configuration of the positioning system allows to perform weld seams in the directions defined by the two linear stages. The positioning system and tungsten rod electrodes (1mm diameter) were used, placing the end of the electrode at 2 mm from the plates, and argon was used as shielding gas, with a typical and constant flow rate of 12 L/min.

Fig. 6 shows a detailed representation of the input optics arrangement. To capture the light radiation produced during the welding process, an optical collimator, orthogonal to the plasma axis, and located approximately at 40 cm from the torch nozzle was used. The end of the collimator was attached to an optical fiber (Ocean

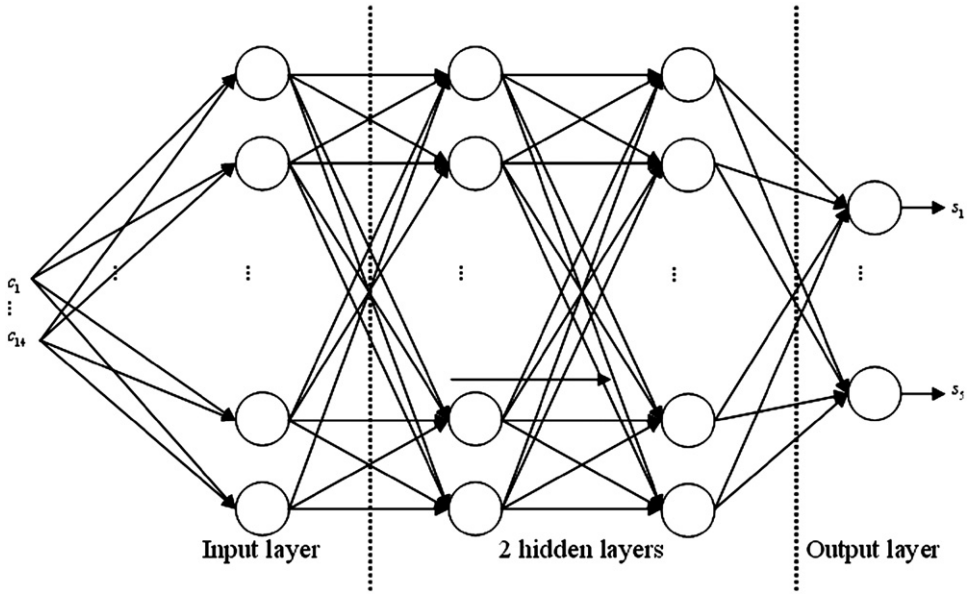

	s_1	s_2	s_3	s_4	s_5
1) Correct welding	1	0	0	0	0
2) Lack of penetration	0	1	0	0	0
3) Low welding intensity	0	0	1	0	0
4) Gas flow reduction	0	0	0	1	0
5) Slight lack of penetration	0	0	0	0	1

Fig. 4. ANN topology and outputs.

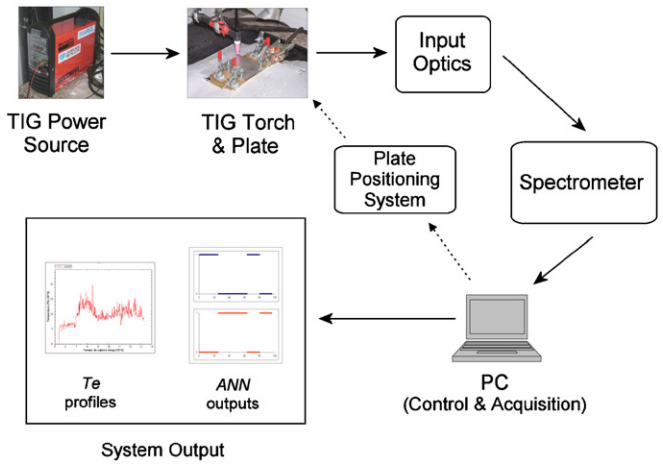

Fig. 5. Experimental welding setup.

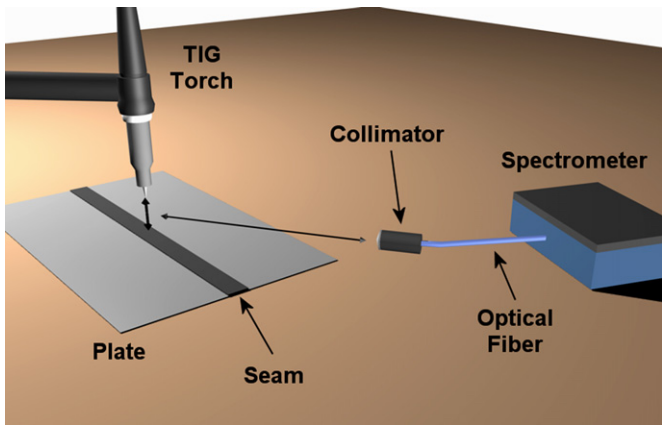

Fig. 6. Input optics arrangement.

Optics P50-UV-VIS). The optical instrumentation also consists of a low-cost, 2048 linear CCD spectrometer (Ocean Optics USB2000). CCD spectrometers are typically formed by an entrance slit, a grating which separates the spectral information of the incoming radiation, and a CCD detector whose pixels will be associated to different wavelengths. The spectral resolution of the selected spectrometer is 0.3 nm, with a spectral range from 195 to 535 nm.

The TIG power source, the spectrometer and the positioning system were controlled by a desktop PC (Pentium IV with a 2 GHz processor), which also performed the processing tasks. To satisfy the real-time, on-line operability criterion, the time consumed in the processing stages should be in the vicinity of the integration time considered in the spectrometer. Tests performed with the ANN implemented in Matlab [17] show that the mean processing time, after the training phase, was

approximately 25 ms. Although with that processing time real-time operability is feasible for the system depicted in Fig. 5, a more efficient implementation of the ANN could be achieved in other programming languages (e.g. C).

A reference welding without defects is presented in Fig. 7, where the welding intensity was kept fixed at 42 A. The top side of the weld seam can be observed in Fig. 7(a), and in (b) the associated T_e profile is depicted. It can be seen that T_e remains constant and without rapid changes along the seam, indicating the absence of possible welding faults. Fig. 7(c) shows the output of the ANN, which in this case corresponds to the activation of the first neuron of the output layer. This neuron is the one associated to a detection of a "correct welding", implying that no defects are to be found in the weld seam. When a defect occurs, this first neuron is deactivated, and the neuron associated to the presence of each particular defect will be activated. It is worth noting that the activation of a neuron means that its output has exceeded a selected threshold. In the tests performed, the threshold was chosen to be 0.5 (see Fig. 7(c)), but the modification of this parameter can be useful when dealing with different quality requirements.

Various experiments were performed trying to provoke visible defects along the weld seam. In Fig. 8(a) the bottom

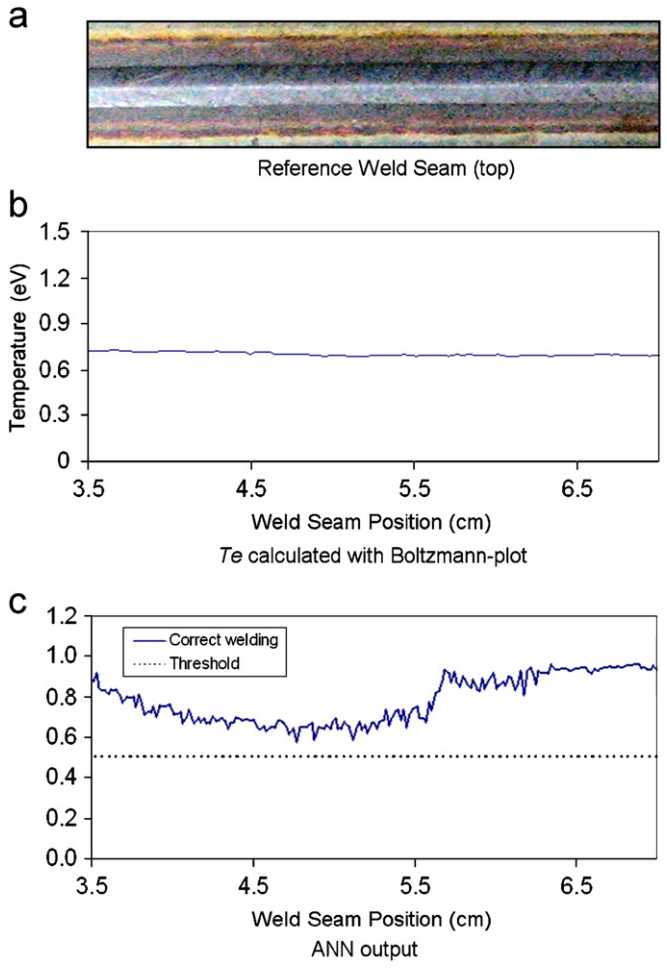

Fig. 7. Reference weld: T_e and ANN output.

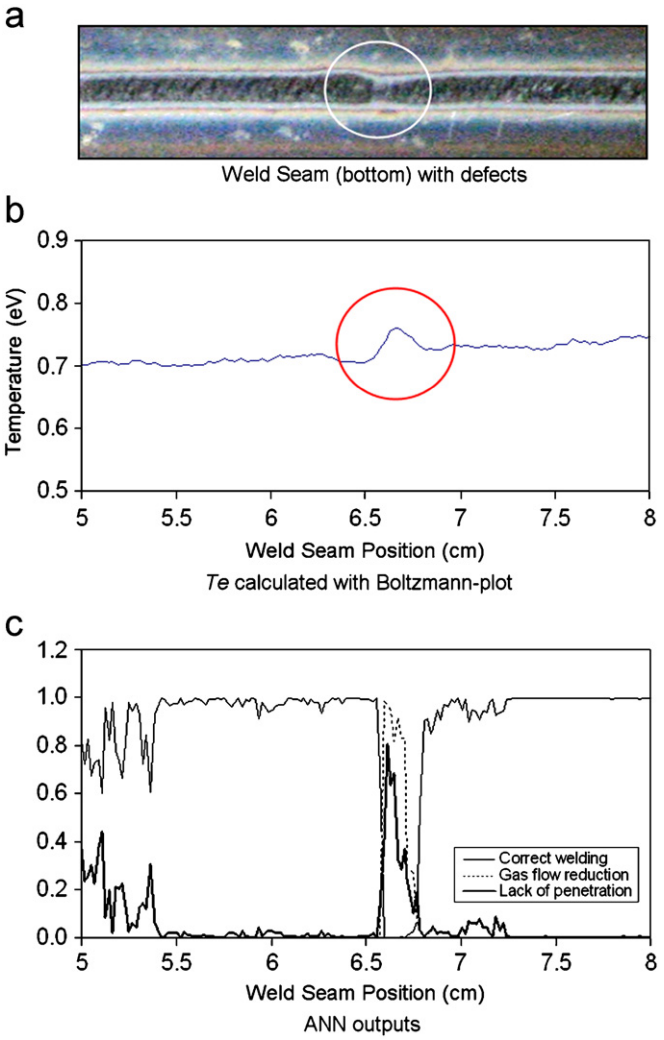

Fig. 8. Detection and classification of weld fault.

side of a weld with a small discontinuity at $x \approx 6.5$ cm is depicted. The defect was caused by a reduction in the shielding gas flow from 12 to 6 L/min, while the welding intensity was kept fixed at 42 A. Fig. 8(b) shows the T_e profile, determined by means of the so-called *Boltzmann-plot* (Eq. (3)) with Ar II lines located at 459, 461, 473, 485 and 488 nm. It can be seen that the defect is clearly detected in the T_e graph at $x \approx 6.5$ cm, where a peak appears. The T_e profile associated to the zones of the weld seam without defects does not exhibit apparent changes, and its value remains constant at approximately 0.7 eV. In Fig. 8(c) the outputs of the ANN are presented. A correlation between the weld seam and these outputs exists, as it can be seen that the defect is clearly identified. While the "correct welding" output is activated along the rest of the weld seam, at $x \approx 6.5$ cm this neuron is deactivated (its value falls to values less than 0.5). At that same point, the output neuron detecting a reduction in the gas flow is activated (dashed line), implying that the system is able to detect the fault and successfully classify its cause. The "lack of penetration" output is also activated in the same point

(thicker line), as the visible effect of the gas flow reduction in the weld seam is precisely a discontinuity or lack of penetration.

The bottom of another faulty weld seam is shown in Fig. 9. In this case, both the welding intensity (42 A) and the gas flow rate (12 L/min) were kept fixed. However, the first part of the weld seam, up to $x \approx 4$ cm is clearly not correct. This was caused by the bend of the plate provoked by previous seams performed in the same plate, which increased the distance between the electrode end and the plate. It can be seen that no change is to be found in the T_e profile (determined with the same Ar II lines used in Fig. 8(b)) in this case, although the discontinuity in the weld seam in $x \approx 4.75$ cm is detected in Fig. 9(b). However, the ANN is able to detect the first part of the weld seam as non-correct, because in Fig. 9(c) the "correct welding" neuron is not activated up to $x \approx 4$ cm. The ANN classifies the fault as a "*lack of penetration*". It is worth noting that, although the value of this output should be next to 1 from the beginning of the weld, the fluctuation in its value from $x = 1$ to 2 cm is associated to the initial instability of the welding process. As the weld seam starts to be distinguishable, the value of the detection of the defect descends, reaching the threshold value of 0.5 at $x \approx 3.15$ cm.

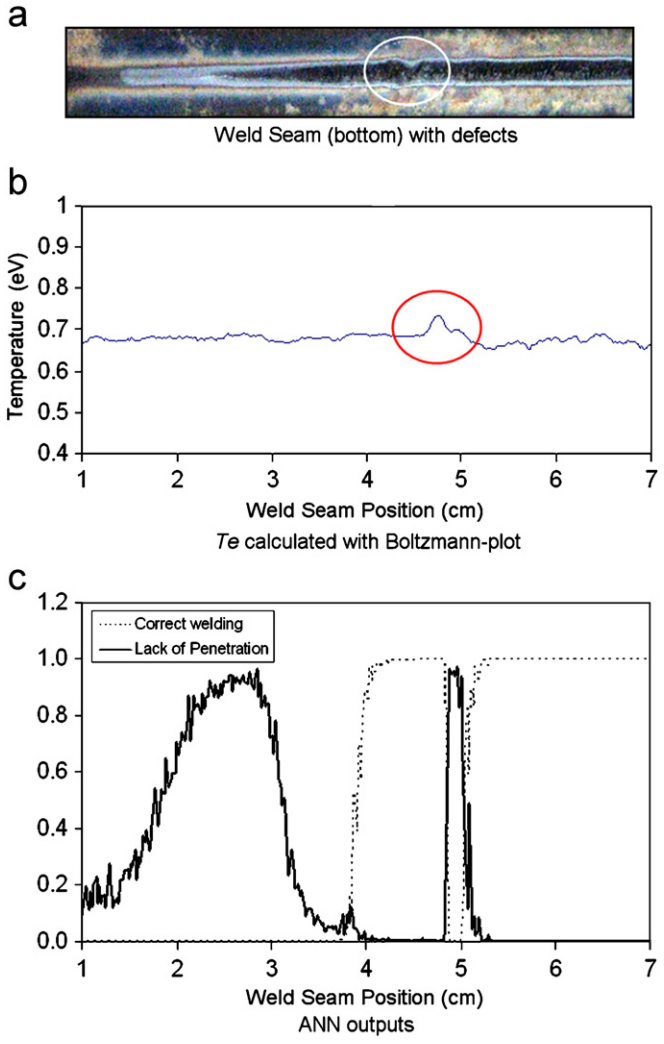

Fig. 9. Weld faults detection by means of ANN.

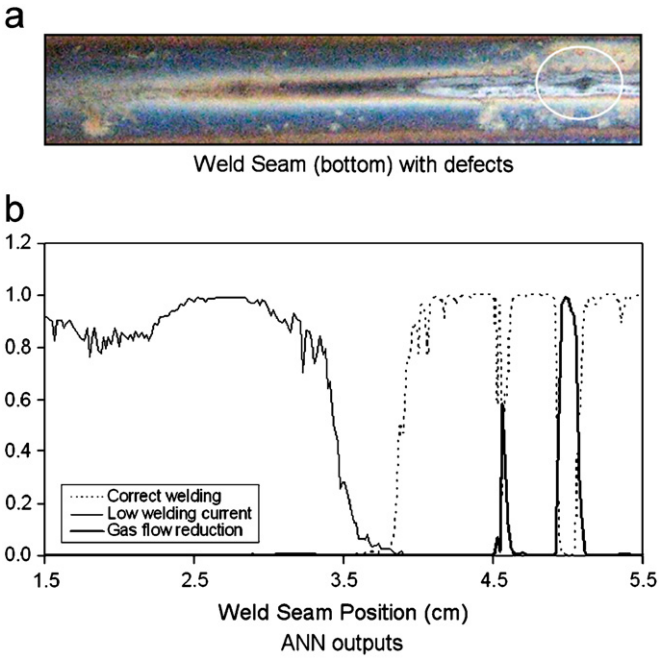

Fig. 10. Low welding current and gas flow reduction identification.

Another example of a flawed seam is presented in Fig. 10. In this case the welding intensity was selected to be 37 A. Again, the bent in the initial part of the plate and the low intensity prevented the seam from forming up to $x \approx 4$ cm (Fig. 10(a)). In Fig. 10(b) can be observed that the low welding intensity is detected by means of the activation of its corresponding neuron. At $x \approx 4$ cm the ANN starts to consider the welding as correct, but in $x = 4.5$ and 5 cm the system detects two defects as caused by gas flow reductions. It should be mentioned that, although a gas reduction from 12 to 2 L/min was performed in $x = 5$ cm, the defect detected at $x = 4.5$ cm seems to be an incorrect defect assignment of the ANN. This can be provoked by the instability of the test, whose insufficient welding current kept the seam from being completely formed.

5. Conclusions

In this paper, a specifically designed artificial neural network has been successfully used in an arc-welding monitoring system as the spectral interpretation algorithm. Besides, the computational performance of the ANN has been enhanced with the application of the PCA analysis to the spectra, prior to the classification in the net. Several examples of weld seams have been presented showing that, once the ANN has been properly trained, it can efficiently discriminate different welding defects, lack of penetration and gas flow reduction among others. Electronic temperature profiles have been also obtained, showing their good agreement with the results provided by the ANN.

It should be mentioned that, although the feasibility of the proposed technique has been demonstrated, the performance of the system could be improved. Gas flow reduction and low welding current have been labeled as different defects from lack of penetration. Actually, when a gas flow reduction or a low welding current occurs it causes a lack of penetration. Considering only the causes of the defects but not their effects, could provide a more suitable topology of the neural network depending on the particular application. Besides, some other more subtle defects like porosities could be considered. Further studies concerning a different defect classification, the application of the proposed strategy of classification by means of PCA and ANN to the T_e profiles, and the evaluation of other discriminant techniques like Fisher are in progress.

Acknowledgments

This work has been co-supported by the Spanish TEC'2004-05936-C02 and TEC'2005-08218-C02-02 projects.

References

[1] Wu CS, Ushio M, Tanaka M. Analysis of the TIG welding arc behaviour. Comput Mater Sci 1997;7:308–14.
[2] Cary HB. Modern welding technology. New Jersey: Prentice Hall; 1989.
[3] Yuang SC, Tarng YS, Lii HR. A comparison between the back-propagation and counter-propagation networks in the modeling of the TIG welding process. J Mater Process Technol 1998;75:54–62.
[4] Ill-Soo K, Joon-Sik S, Sang-Heon L, Yarlagadda PKDV. Optimal design of neural networks for control in robotic arc welding. Robotics Computer-Integrated Manuf 2004;20:57–63.
[5] Di L, Srikanthan T, Chandel RS, Katsunori I. Neural-network-based self-organized fuzzy logic control for arc welding. Eng Appl Artif Intell 2001;14:115–24.
[6] Ferrara M, Ancona A, Lugara PM, Sibilano M. On-line quality monitoring of welding processes by means of plasma optical spectroscopy. Proceedings of SPIE, 2000. p. 3888.
[7] Szymanski Z, Kurzyna J. Spectroscopic measurements of laser induced plasma during welding with CO_2 laser. J Appl Phys 1994; 76:7750–6.
[8] Vincenzo DR, Bruno B, Franco C. Defect detection in stainless steel uranus 45 TIG-welded joints by acoustic emission. Mater Evaluation 1987;45:348–52.
[9] Wang JJ, Lin T, Chen SB. Obtaining weld pool vision information during aluminium alloy TIG welding. Int J Adv Manuf Technol 2005;26:219–27.
[10] Hong L, Hao Z, Lunji H, Xiyuan H, Zhude Z. Application of artificial neural network in laser welding defect diagnosis. J Mater Process Technol 2005;170:403–11.
[11] Griem HR. Principles of plasma spectroscopy. Cambridge: Cambridge University Press; 1997.
[12] Workman Jr J, Springsteen AW. Applied spectroscopy: a compact reference for practitioners. London: Academia Press Limited; 1998.
[13] Chen CH. Fuzzy logic and neural networks handbook. New York: McGraw-Hill; 1996.
[14] Girosi F, Makhoul J, Manolakos E, Wilson E. Neural networks for signal processing V. Proceedings of the 1995 IEEE workshop, 1995.
[15] Lay D. Linear algebra and its applications. New York: Addison – Wesley; 2000.
[16] Jackson JE. A users guide to principal components. New York: Wiley series in Probability and mathematical statistics; 1991.
[17] Mathworks, Inc., Neural network tool box user's guide. Verso 4.0, MA, USA: Natick; 2001.